Impact of Precipitation on Ocean Responses during Tropical Cyclone

Fu Liu,[a] Ralf Toumi,[b] Han Zhang,[c,d] Dake Chen,[c,d,e]

[a] *School of Atmospheric Sciences, Sun Yat-sen University, Zhuhai, China*

[b] *Department of Physics, Imperial College of London, London, United Kingdom*

[c] *State Key Laboratory of Satellite Ocean Environment Dynamics, Second Institute of Oceanography, Ministry of Natural Resources, Hangzhou, China*

[d] *Southern Marine Science and Engineering Guangdong Laboratory (Zhuhai), Zhuhai, China*

[e] *School of Oceanography, Shanghai Jiao Tong University, Shanghai 200030, China*

Corresponding author: zhanghan@sio.org.cn

ABSTRACT

Precipitation plays a crucial role in modulating upper ocean salinity and the formation of barrier layer, which affects the development of tropical cyclones (TCs). This study performed idealized simulations to investigate the influence of precipitation on the upper ocean. Precipitation acts to suppress the wind-induced sea surface reduction and generates an asymmetric warming response with a rightward-bias. There is substantial vertical change with a cooling anomaly in the subsurface, which is about three times larger than the surface warming. The mean tropical cyclone heat potential is locally increased but the net effect across the cyclone footprint is small. The impact of precipitation on the ocean tends to saturate for extreme precipitation, suggesting a non-linear feedback. A prevailing driver of the model behavior is that the freshwater flux from precipitation strengthens the stratification and increases current shear in the upper ocean, trapping more kinetic energy in the surface layer and subsequently weakening near-inertial waves in the deep ocean. This study highlights the competing role of TC precipitation and wind. For TC is weaker than Category 3, the warming anomaly is caused by reduced vertical mixing, whereas for stronger TCs, the advection process is most important.

1.Introduction

The interaction between tropical cyclones (TCs) and the upper ocean is a complex process that influences both the TCs' development and the ocean's characteristics. The vast warm upper ocean provides abundant energy needed for a TC to form and strengthen in the form of the heat flux exchange (Emanuel 1995). As a TC moves over the ocean, the strong cyclonic wind can increase turbulence and vertical entrainment in the upper layer, which brings cold deep water to the surface, results in a reduction in sea surface temperature and leaves a cold wake which biased to the right side of track in the northern Hemisphere (Price 1981; Cione and Uhlhorn 2003; Zhang 2023). In turn, the resultant sea surface temperature (SST) cooling subsequently has negative feedback on TCs' intensity by suppressing the exchange of air–sea enthalpy fluxes (Xu and Wang 2010; Lloyd and Vecchi 2011).

The SST responses to TCs were modulated by both the thermal and salinity stratification of the upper ocean (Wang et al. 2011; Neetu et al. 2012; Domingues et al. 2015; Rudzin et al. 2017, 2019; Zhang et al. 2021; Jarugula and McPhaden 2022). Recently, studies highlighted the effect of the salinity stratification on the modulation of vertical entrainment (Balaguru et al. 2016; Yan et al. 2017; Hlywiak and Nolan 2019). When there is strong salinity stratification within the surface isothermal layer, i.e., a barrier layer, the SST cooling tends to be suppressed due to the weaker vertical entrainment that is inhibited by a stable stratification (Balaguru et al. 2012). Using Argo measurements and a diagnostic mixed layer model, a reduction of 0.4-0.8 ℃ in SST cooling was found when a TC passed over a barrier layer with a thickness of 5–15 m (BL, Wang et al. 2011). For a strong TC which is strong enough to provide sufficient turbulent kinetic energy (TKE) into upper ocean to penetrate into the BL with warm water, the heat loss and SST cooling can be partly compensated by the warm water in the BL (Yan et al. 2017). Observations and model studies have revealed that TC intensification rates can be significantly higher over regions with barrier layers

(Balaguru et al. 2012; 2016; 2020).

Many studies based on observations and numerical models have emphasized the importance of precipitation (Bond et al. 2011; Jourdain et al. 2013; Jacob and Koblinsky 2007; Liu et al. 2020) and river input (Newinger and Toumi 2015) on the upper ocean salinity stratification. The influx of freshwater reduces the density of the surface water and strengthens the salinity stratification, suppresses vertical mixing and forms of a shallow, stable mixed layer, which inhibits the exchange of heat and nutrients between the surface and deeper layers. Therefore, TC precipitation acts to reduce the mixed layer depth after the TC passage, hence reducing cold water entrainment (Bond et al. 2011; Liu et al. 2020). Several studies have found that the upper-ocean salinity stratification in the Western tropical Pacific has a strengthening tendency under global warming, which is the result of the increasing freshwater flux related to relative stronger precipitation (Held and Soden 2006; Wentz et al. 2007; Cravatte et al. 2009; Durack et al. 2012). Exploring the TC precipitation-induced upper ocean responses is noteworthy to understand the evolution of upper ocean stratification, especially under the background of global warming.

There have been a few studies that specifically focusing on the effect of TC precipitation on the upper ocean. It has been found that precipitation can enhance the upper ocean stability (Jacob and Koblinsky 2007; Huang et al. 2009; Jourdain et al. 2013; Steffen and Bourassa 2020), alert the upper ocean current (Jacob and Koblinsky 2007) and increase the current shear in upper ocean (Steffen and Bourassa 2020). Using the Hybrid Coordinate Ocean Model (HYCOM), Jacob and Koblinsky (2007) found that the SST cooling was weakened by about +0.2~0.5 ℃ after including the TC precipitation in the atmospheric forcing field. Huang et al. (2009) also demonstrated that neglecting precipitation in simulations of TC-ocean interaction may lead to an overestimation of the surface cooling, although it is of negligible significance. Jourdain et al. (2013) showed that heavy precipitation of TC can result in a slightly but not negligible reduction of the cold wake, with a median of 0.07 K for a median 1 K cold wake. Lately, another case study using the Regional Ocean Modeling System (ROMS) showed that the precipitation forcing can induce both warming and cooling SST anomalies at the same time of about ± 0.3℃ (Steffen and Bourassa 2020). Research in the context of global warming also shows that ‘freshening of the upper ocean, caused by greater precipitation in places where typhoons form, tends to intensify super typhoons by reducing their ability to cool the upper ocean (Balaguru et al. 2016).

Given that previous studies primarily focused on the sea surface responses in real TC cases (Jacob and Koblinsky 2007; Huang et al. 2009; Jourdain et al. 2013; Steffen and Bourassa 2020), the effect precipitation was be coupled with complex ocean processes and the vertical responses to precipitation forcing was less studied. Thus, we choose to use idealized model configuration to make things clear and help eliminate the disparities between real TC cases. Regarding the role of TC precipitation on the TC-induced upper ocean responses, the following specific questions will be addressed in this study:

(1) Is the precipitation-induced SST variation symmetric?

(2) What is the impact on the sub-surface and on the ocean heat content? Can we expect a non-negligible effect of precipitation on the upper ocean heat content?

(3) Is the precipitation-induced response linear facilitating a positive feedback route or not?

(4) Does the precipitation act similar under different TC intensities?

This paper is organized as follows: Section 2 described the model configuration, numerical experiments and the datasets used for model simulation in detail are described. Section 3 presents the detailed results, including the three-dimensional structure of oceanic responses, the budget analysis, the nonlinear relationship between ocean responses and precipitation forcing, and the dynamic mechanisms are presented.

Finally, Section 4 gives a brief conclusions and discussions, as well as the limits of this study.

2. Method and Model description

a. Oceanic parameters

Following the definition in Kara et al. (2000), the mixed layer depth is defined as the depth at which the density difference between this level and the density at 10 m layer exceeds a specific threshold. This threshold is calculated by using the following equation:

$$\Delta\sigma = \sigma(T_{10} - 0.5°\mathrm{C}, S_{10}, 0) - \sigma(T_{10}, S_{10}, 0) \qquad (1)$$

where T_{10} and S_{10} indicate the temperature and salinity at 10 m depth, σ is water density.

The ocean heat content (OHC) is calculated by the following method:

$$Q = \int_{z_1}^{z_2} \rho C_p T dz \qquad (2)$$

where Q is ocean heat content, ρ is water density in model output, T is water temperature, z_1 and z_2 are the top and bottom of water layer chosen to calculate the heat content, C_p is specific heat capacity for water and we take C_p as 4200 $J \cdot kg^{-1} \cdot °\mathrm{C}$ for simplicity. Two types of OHC are calculated in this study: one is the total heat content of the water column above 100 m depth, i.e., OHC_{100}; the other is the tropical cyclone heat potential (TCHP), which is the summation of OHC from the surface to the depth of the 26 °C isotherm (Leipper and Volgenau 1972).

Near-inertial waves (NIWs) are a dominant mode of high-frequency variability induced by TC wind forcing, which appear as a prominent peak near the inertial frequency in the internal wave spectrum (Alford et al. 2016). We applied a fourth-order Butterworth filter in the time series of original simulated current to extract the signal of near-inertial current. The upper and lower limits for the filter are set at

$0.80f$ *and* $1.13f$ (Guan et al. 2014), respectively. Here, f is the Coriolis parameter, which remains constant throughout the entire model domain. Then the current shear and the kinetic energy of near-inertial waves (NIKE) are calculated as follows:

$$S^2 = (\partial u/_{\partial z})^2 + (\partial v/_{\partial z})^2 \qquad (3)$$

$$NIKE = \frac{1}{2}\rho({u_i}^2 + {v_i}^2) \qquad (4)$$

where u and v are the horizontal components of current, the subscript i indicates the component of near-inertial waves.

b. Idealised precipitation model

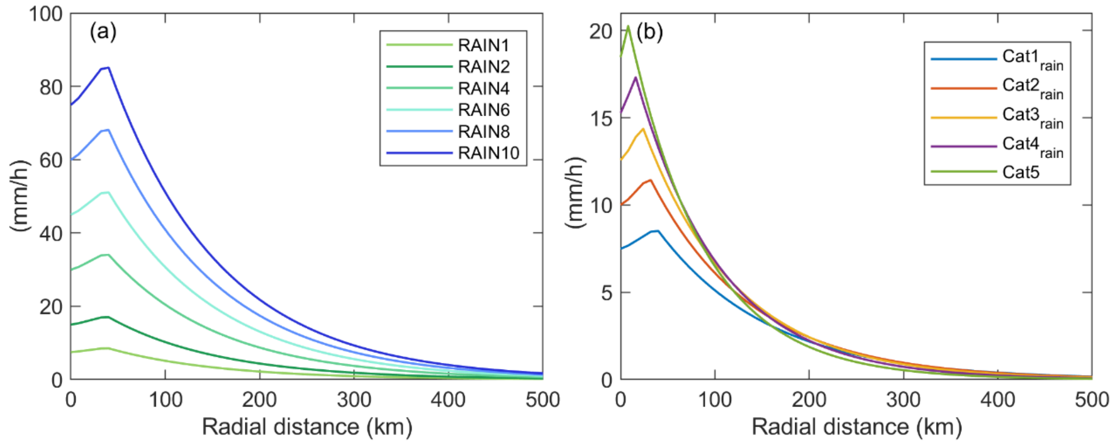

FIG. 1. The radial profile of precipitation rate in (a) 6 experiments with varied wind and precipitation intensity. Note that the precipitation in ‘RAIN1’ is same with ‘Cat1_rain’.

The symmetric precipitation forcing field for numerical simulations is created by using the ideal precipitation model created by the Precipitation Climate and Persistence Model (R-CLIPER) (Tuleya et al. 2007). The modeled TRMM (Tropical Precipitation Measuring Mission) R-CLIPER profile is capable to reproduce the climatological rain rate (Tuleya et al. 2007; Lu et al. 2022). In TRMM R-CLIPER, the rain rate is defined as a function of radius (r) and the maximum wind (V_{max}), with the precipitation decreased linearly from the radius of maximum rain rate (r_m) to the eye and then decays exponentially outside the r_m:

$$Rain\ rate\ (r, V) = \begin{cases} P_0 + (P_m - P_0)\frac{r}{r_m}, & r < r_m \\ P_m exp(-\frac{r - r_m}{r_e}), & r \geq r_m \end{cases} \quad (5)$$

where the P_0 is the rain rate at r=0 and P_m is the maximum rain rate at r=r_m. The four parameters in Eq.5 are correlated with V_{max} of vortex:

$$\begin{cases} P_0 = a_1 + b_1 * (1 + (V_{max} - 35)/33) \\ P_m = a_2 + b_2 * (1 + (V_{max} - 35)/33) \\ r_m = a_3 + b_3 * (1 + (V_{max} - 35)/33) \\ r_e = a_4 + b_4 * (1 + (V_{max} - 35)/33) \end{cases} \quad (6)$$

The values for 8 constants ($a_1 - a_4, b_1 - b_4$) in Eq.6 are same with the values used by the National Hurricane Center (NHC) in Table 2 of Tuleya et al. (2007). Please see Tuleya et al. (2007) to get the exact value for 8 constants in Eq.6. Fig. 1 shows the radial profiles in our numerical experiments.

c. Model configuration

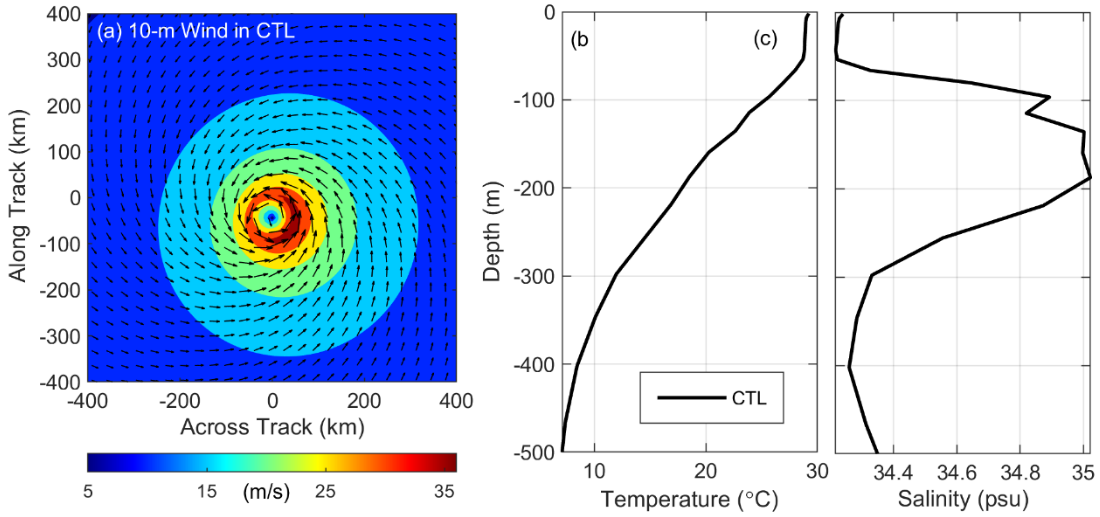

FIG. 2. The (a) horizontal map of 10-m wind field in CTL run, and the initial vertical profile of (b) temperature and (c) salinity for the ocean model.

To focus on the effect of precipitation on oceanic responses, only the oceanic model, ROMS (Shchepetkin and McWilliams 2005), is used in this study. Furthermore, idealised experiments are conducted to isolate the effect of precipitation from the complicated background ocean conditions. The model domain is roughly 2000 km, and 3500 km in the cross-track direction and along-track direction, respectively. In the vertical direction, a 40-level stretched terrain-following coordinate is used with the vertical stretching parameters θs, θb, and Tcline set to 6.5, 2.5, and 150 m, respectively. The horizontal resolution is approximately 8 km and the time step of the simulation is 60 s. The vertical mixing closure scheme is the generic length-scale (GLS) parameterizations which implements a tunable set of length scale equations (Warner et al. 2005) and has been widely used to study the TC-ocean interaction (Steffen and Bourassa 2020; Wu et al. 2021).

The model starts from a stationary state which merely has initial temperature, salinity and density, but no background current. Note that the initial field is homogenous in horizontal direction. The surface fluxes, 2-m air temperature and 2-m relative humidity are provided by the analytical field embedded in ROMS. Then the model is triggered by idealized wind and precipitation forcing field. We use the Rankine Vortex model to create an asymmetric wind field of a TC vortex (Huges 1952), which has a maximum wind speed of 35.7 m/s (reaches a typhoon category) and a radius of maximum wind (RMW) of 50 km. The idealized TC moved from south edge to north edge along the center of model domain at a translation speed of 6 m/s. The coefficient for Rankine vortex is defined as 0.5 in this study. Note that the idealized simulations are performed on a f-plane at 20°N to avoid the β-effect (Madala and Piacsek 1975).

TABLE 1. Details of 7 experiments with different precipitation forcing but same wind forcing. Please note that the 'CTL' ('RAIN1') run is also the 'Cat1_norain' (Cat1_rain) in Table2.

Run	Initial condition	Peak rain rate (mm/h)	Aim
CTL		No	

RAIN1		8.5	
RAIN2		2*8.5	
RAIN4	Same as CTL	4*8.5	Examine the influence of precipitation
RAIN6		6*8.5	
RAIN8		8*8.5	
RAIN10		10*8.5	

In total, 15 idealised experiments are performed. Firstly, the ROMS is driven by an idealised category 1 TC (maximum wind speed is 35.7 m/s) without precipitation and freshwater flux (hereafter referred to as the ‘CTL’ and ‘Cat1_norain’), which can show us the dynamic effect of TC wind forcing. To explore the linear/nonlinear correlation between precipitation and precipitation-induced SST variations, we conducted other 6 experiments by enlarging the rain rate by up to a factor of 10 while keep the wind forcing same. The only difference among these experiments is the amount of precipitation forcing, with the precipitation intensified from normal precipitation to 2, 4, 6, 8, and 10 times of the normal precipitation. The peak rain rate is 8.5 mm/h for the base case with rain (RAIN1, Fig. 1b). Even this highest rain rate in RAIN10 (85 mm/h) is physically plausible and close to some observations (Chang et al. 2014; Lu et al. 2022). For example, the peak hourly precipitation recorded by gauge station reaches 131 mm during Supertyphoon Rammasun (2014) (Lu et al. 2022), which is 15 times the base rain rate in RAIN1 (also called as ‘Cat1_rain’). In addition, the highest localized rain rate recorded during Cyclone Sidr (2007) was 83.46 mm/h (Chang et al. 2014), which is close to the precipitation in RAIN10. With this approach of holding the wind speed constant while varying precipitation, we can clearly isolate the role of precipitation. Fig. 1a shows the radial profile of these experiments.

Table 2. Initial vortex intensity and precipitation rate for 10 experiments with varied TC intensity. Note that the ‘Cat1_norain’ (‘Cat1_rain’) is same with ‘CTL’ (‘RAIN1’) in Table1.

Exps	Cat1	Cat2	Cat3	Cat4	Cat5

	_rain	_norain	_rain	_norain	_rain	_norain	_rain	_norain	_rain	_norain
Maximum Wind (m/s)	35.7		45.5		55.3		65.2		75.0	
Peak Rain (mm/h)	8.5	0	11.5	0	14.4	0	17.4	0	20.4	0

Given that the precipitation tends to increases with TC intensity (Lonfat et al. 2004; Alvey et al. 2015), another 8 experiments are conducted with TC intensity and precipitation rate vary from category 2 to category 5 to simulate a more realistic upper ocean response. The precipitation rate for different TC intensities is obtained from the TRMM R-CLIPER model. Note that the RMW remains 50 km for all experiments. Fig. 1b shows the radial profile of idealized precipitation rate under 5 TC categories.

3. Results

a. Sea Surface responses

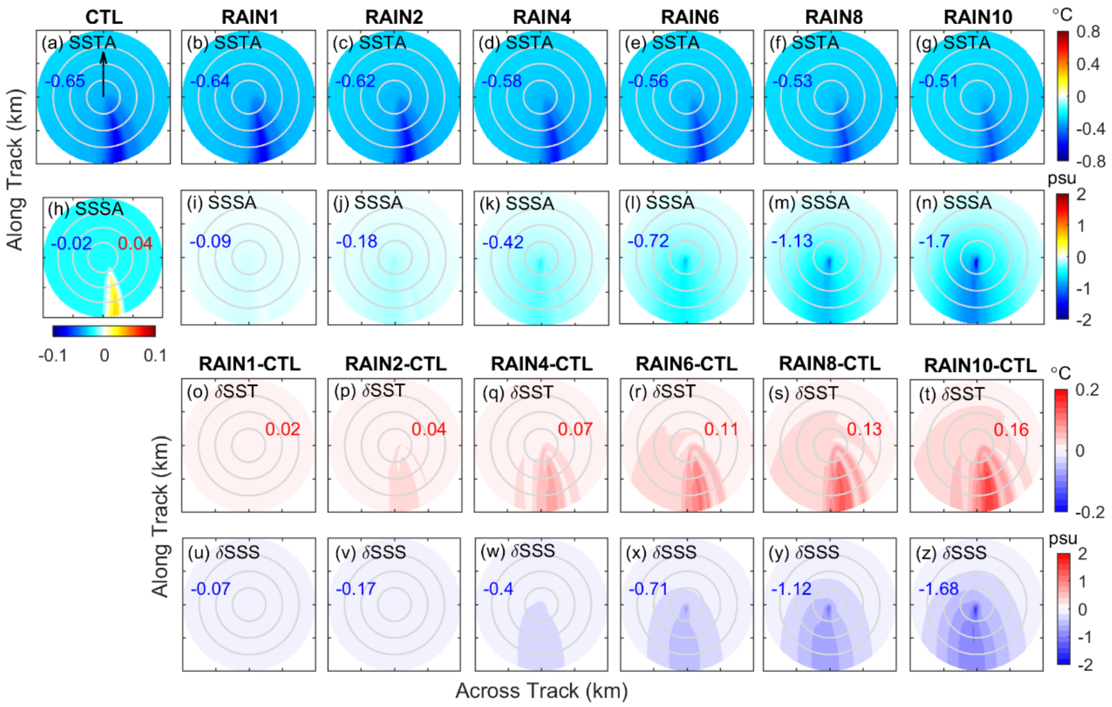

FIG. 3. Horizontal map of (a-g) SST anomalies, (h-n) SSS anomalies, (o-t) difference of SST anomalies, and (u-z) difference of SSS anomalies in a vortex-relative coordinate. The anomalies in (a-n) are relative to the initial condition. The difference in (o-z) is the difference between 6 runs with precipitation forcing and the CTL run without precipitation forcing. The distance between gray circles is 100 km. The blue (red) numbers in each panel show the maximum negative (positive)value, i.e., the

strongest cooling/fresh (warming/salty) signal. Only results within a radius of 400 km are plotted.

Fig. 3a-n displays the horizontal map of SST anomalies (SSTA) and sea surface salinity anomalies (SSSA) after the TC vortex has passed by. Similar to previous studies (Price 1981; Zhang et al. 2021), the sea surface responses to TC vortex in CTL run are dominated by the wind forcing, leaving a rightward-biased SST cooling and SSS increasing responses. This is attributed to the rightward-biased vertical mixing, which entrains cold and salty water upward to mix with the warm and fresh water in mixed layer. The sensitivity of the response to the amount of precipitation can be seen in Fig. 3o-z. Adding precipitation causes stronger SSS freshening and weaker SST cooling i.e., results in a relative warming. The results of idealized runs show a homogeneous precipitation-induced relative warming within a radius of 400 km around the TC center, with the maximum biased to the right side of track (Fig. 3o-t). Note that the precipitation-induced warm wake was almost overlapped with the wind-induced cold wake (Fig. 3a), suggesting the inhibition of precipitation on the cold wake. The maximum precipitation-induced SST warming in RAIN1 and RAIN10 is about 0.02 ℃ and 0.16 ℃, respectively. The precipitation induces a nearly symmetrical freshening anomaly on both sides of TC track, which slightly biased to the left side. The rightward biased warming and leftward biased freshening induced by precipitation indicate the different dominant mechanisms behind the SST and SSS responses. For SSS, precipitation has a comparable importance with the dynamic processes, while the SST is still dominated by the rightward vertical mixing and the precipitation acts indirectly by modulating the dynamical processes.

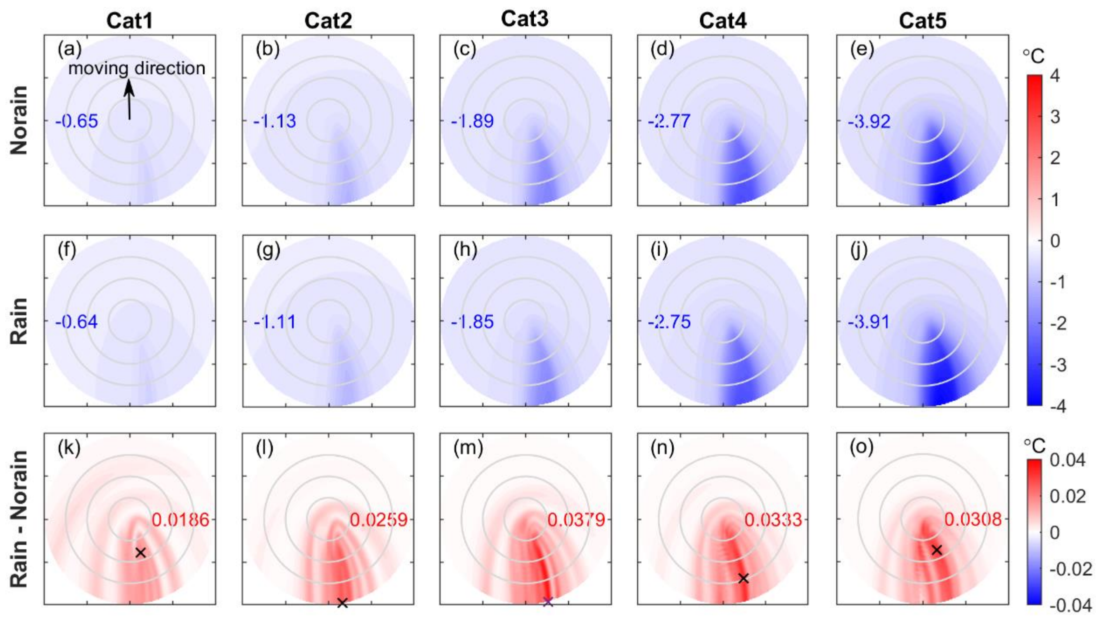

FIG. 4. Similar to FIG. 3, but for results from experiments with varied TC intensities and precipitation forcing. The blue numbers in (a-j) and red numbers in (k-o) show the strongest SST cooling and relative-warming signal, respectively. Only results within a radius of 400 km are plotted.

Fig. 4 shows the averaged SSTA during the whole simulation period and the difference in SSTA between experiments with precipitation forcing and without precipitation forcing. The SSTA enhanced as TC intensified (Price 1981; Zedler et al. 2002; Black and Dickey 2008; D'Asaro et al. 2007; Reul et al. 2020), regardless of whether the freshwater flux was considered. The relative-warming induced by precipitation occupied the entire region within 400 km for both weak and strong TCs (Fig. 4k-o). The relative warming also shows a rightward bias that similar to Fig. 3. Initially, the precipitation-induced warming intensified from 0.019 °C in Cat1 to 0.038 °C in Cat3, and then decreased slightly with TC wind increased. Even the highest value of 0.038 °C in Cat3 is only 2% (0.038 °C v.s. 1.89 °C) of the wind-induced SSTA (Fig. 4c). In addition, the precipitation-induced SST warming in Cat 5 is only 0.8% of the wind-induced SSTA (Fig. 4e, o) since the wind-induced SSTA is much stronger. Here we can answer the first question about the symmetry of precipitation-induced responses. Without the complicated background oceanic condition, the freshwater flux from precipitation can weaken the wind-induced SST cooling, cause a rightward-biased relative warming signal that occupied the region within 400 km. This warming signal and asymmetry remain valid in extreme precipitation events and in strong TC cases.

b. Vertical profiles

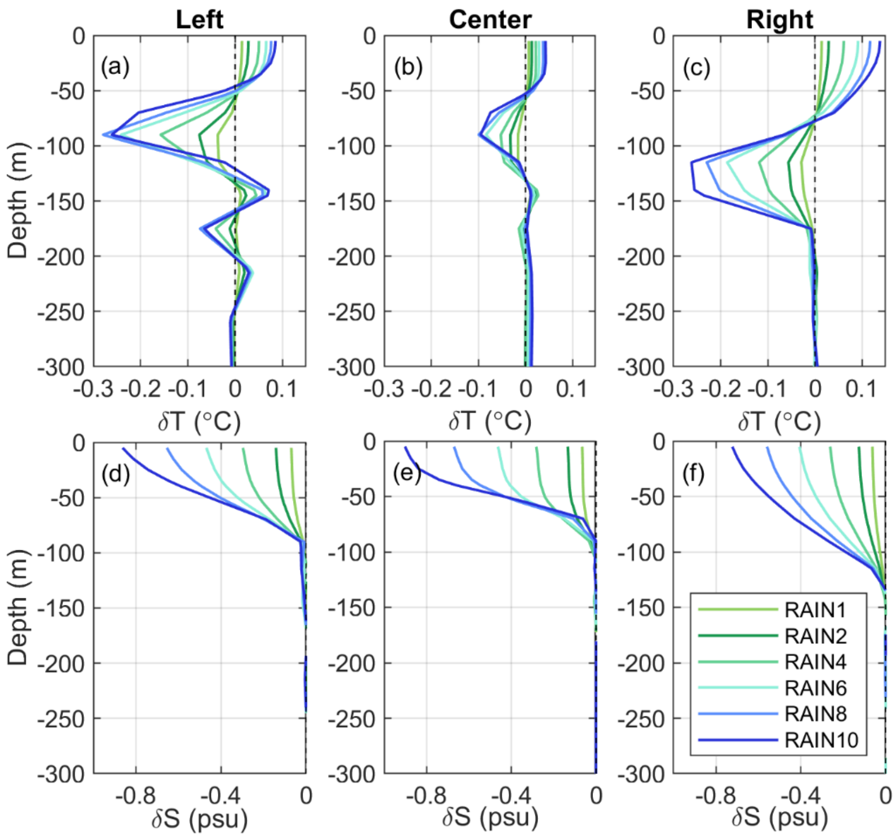

FIG. 5. Vertical profiles of the differences in (a-c) water temperature and (d-f) salinity induced by precipitation at three points: (a, d) the point at a radius of RMW at the left side of TC center (i.e., P_{left}); (b, e) the point at TC center (i.e., P_{center}); and (c, l) the point at a radius of RMW at the right side of TC center (i.e., P_{right}). The profiles were averaged from the arrival time of TC to 1.5 days after TC passed by, which represents the forced stage. The colored lines represent the results in different experiments.

The vertical profiles of precipitation-induced temperature and salinity differences at the left, TC center and right side of TC track were shown in Fig. 5, which shows the vertical structure of the responses during the forced stage. The forced stage lasts for about 1.5 days and corresponds to the period when the local position is directly influenced by the wind of the TC (Price 1994). During this stage, the instant response to precipitation is a warm-cold-warm structure from surface to a depth of 300 m. The mixed layer has a slight warm anomaly but the subsurface layer has a stronger cooling anomaly. Note that the precipitation-induced subsurface cooling was about 3 times of the precipitation-induced SST warming. It is caused by the large vertical temperature gradient and the large vertical advection in subsurface layer. The salinity discrepancies were mainly trapped in the mixed layer (Fig. 5d-f). The temperature discrepancies are more pronounced on the right of the track, whereas the salinity discrepancies are most significant near the TC center and smallest on the right. This is the coupled effect of rightward-biased wind-induced dynamic responses and a symmetric dilution effect of precipitation. The depth at which the maximum subsurface cooling occurs is shallower on the left, which was related to the relatively weaker TC-induced dynamic responses. Regardless of the location, the magnitude of discrepancies induced by precipitation intensified with increasing precipitation amounts.

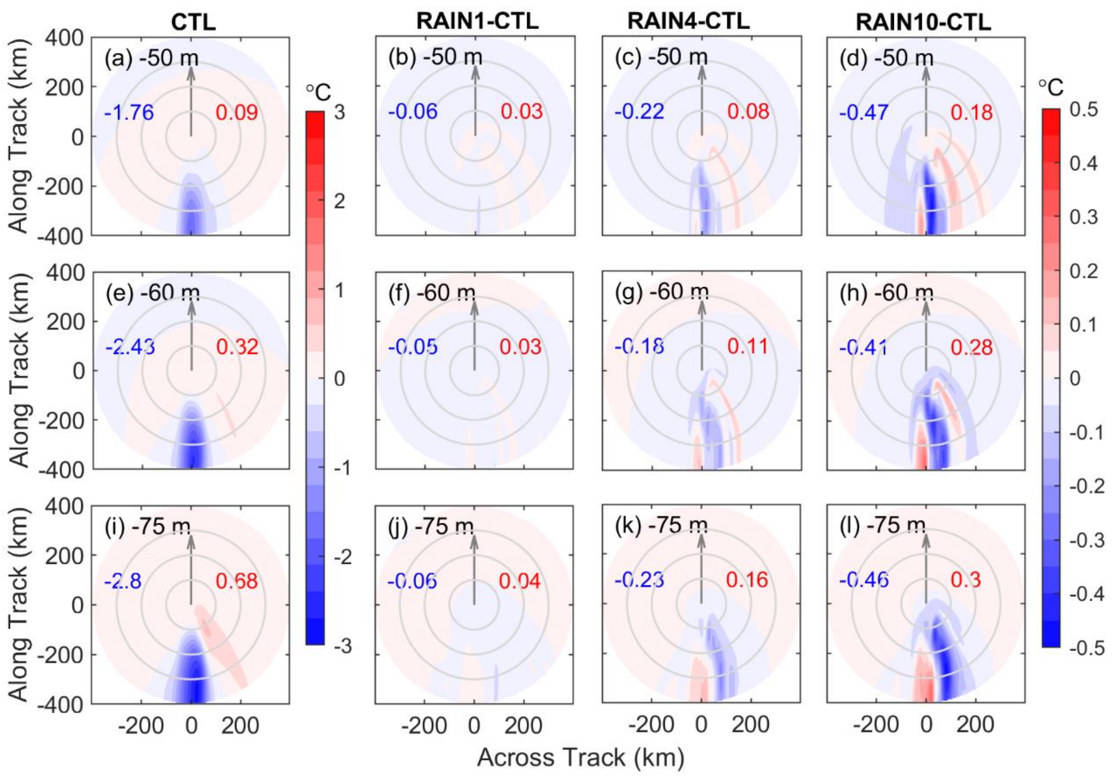

FIG. 6. Horizontal map of the temperature responses in CTL run, and the differences in temperature induced by precipitation at a depth of (a-d) 50 m, (e-h) 60 m and (i-l) 75

m. The first column represents the result in CTL run, and other columns represent the difference between idealized experiments (RAIN1, RAIN4, RAIN10) and the CTL. Each gray circles indicates a distance of 100 km. The gray vector indicates the moving direction of idealized TC vortex. The blue and red numbers in each panel show the maximum positive and negative value, i.e., the largest warming and cooling.

Fig. 6 shows the horizontal map of differences in water temperature at a depth of 50 m, 60 m and 75 m. In CTL, a distinct wake was observed at the subsurface layer. According to Zhang (2023), a pronounced upwelling and cooling was observed near the right in the subsurface layer. As can be seen, the precipitation-induced differences of temperature in the subsurface layer displays a spatial pattern characterized by both positive and negative anomalies. At 50 m depth which is near the base of mixed layer, there is a strong clod anomaly behind TC center, with a tiny warming anomaly occurred between 200-400 km. As the depth increases to 75 m, the warm anomaly expands wider. The magnitude of the subsurface temperature discrepancies is several times larger than those at sea surface, such as -0.06 °C vs. -0.02 °C in RAIN1, -0.47 °C vs. -0.16 °C in RAIN10.

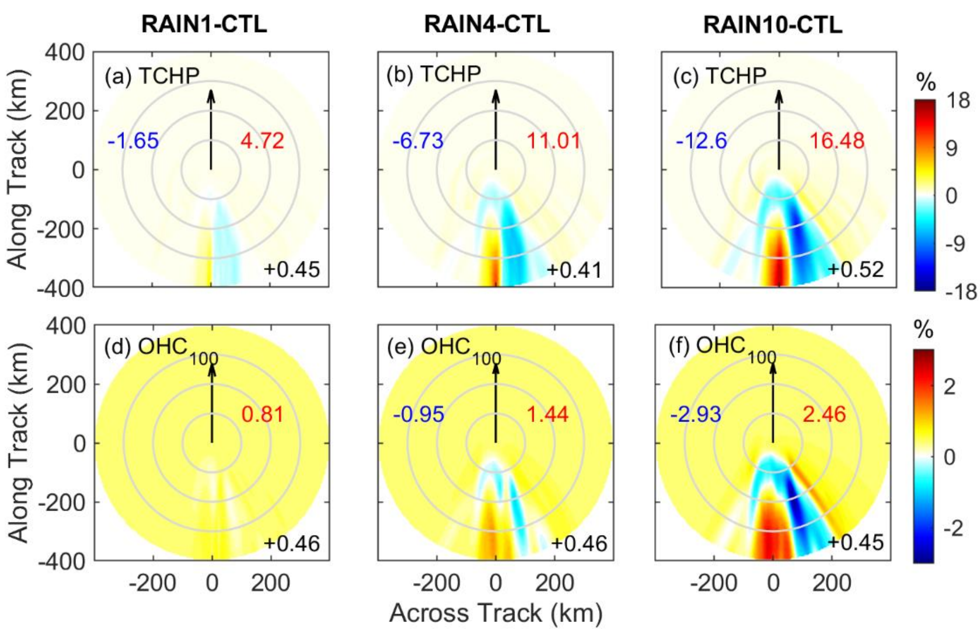

FIG. 7. Horizontal map of the proportion of differences in (a-c) TCHP and (d-f) OHC_{100} induced by precipitation. The proportion is derived from the differences induced by precipitation over the original value of heat content in CTL run. Each gray circles indicates a distance of 100 km. The black vector indicates the moving direction

of idealized TC vortex. The blue and red numbers in each panel show the maximum positive and negative value, i.e., the largest increasing and decreasing signal. The black number at the bottom right corner in each panel represents the azimuthal mean within 400 km from TC center.

Fig. 7 shows the horizontal map of both precipitation-induced TCHP and OHC_{100} anomalies in experiments with same wind forcing bur increasing precipitation forcing. The TCHP and OHC_{100} share a similar spatial pattern, which also resembles the pattern of subsurface temperature discrepancies in Fig. 6. The strongest positive (negative) signals are located at a distance of 200 km from TC center (biased to the right side of track), with a maximum exceeding +4.72% in RAIN1 and +16.48% in RAIN10. Compared to the positive anomaly (i.e., increase), the negative anomaly (i.e., decrease) of heat content is a bit smaller. Considering the total area affected there is almost cancellation of the effect. The azimuthal mean TCHP anomalies within a 400 km range is merely -0.45% in RAIN1, +0.41% in RAIN4, and +0.524% in RAIN10. The azimuthal average of OHC_{100} is similar to TCHP.

To sum up, the subsurface was also modulated by precipitation forcing at a marginally degree. Precipitation can induce a rightward-biased cold anomaly in subsurface, even the upper ocean heat content was modulated. Although the TCHP can be modulated by 4.72 % at peak value, the azimuthal mean over the domain within 400 km was only 0.45 %, which can be negligible.

c. Dynamics

In ROMS, the heat budget equation governs the time evolution of salinity and temperature (http://www.myroms.org/wiki):

$$\frac{\partial C}{\partial t} + \vec{v}\cdot\nabla C = -\frac{\partial}{\partial z}\left(\overline{C'w'} - \nu_\theta \frac{\partial C}{\partial z}\right) + D_C + F_C \qquad (7)$$

The second term in Eq.7 represents the change induced by both horizontal and vertical advection, the first term on the right-hand in Eq.7 reflects the effect of vertical diffusion (i.e., vertical mixing) including molecular diffusivity and turbulent diffusivity. D_C

indicates the horizontal diffusive term, and F_C represents the surface forcing term. For simplicity, the heat budget equation can be written as:

$$T_{rate} = -T_{hadv} - T_{vadv} + T_{hdiff} + T_{vdiff} + Q_s \qquad (8)$$

which means the local tendency rate of temperature (T_{rate}) was determined by the horizontal advection (T_{hadv}), vertical advection (T_{vadv}), horizontal diffusion (T_{hdiff}) and vertical diffusion (T_{vdiff}), as well as the surface heat flux (Q_s). All six terms in Eq.8 are derived directly from the output of ROMS as diagnostic variable.

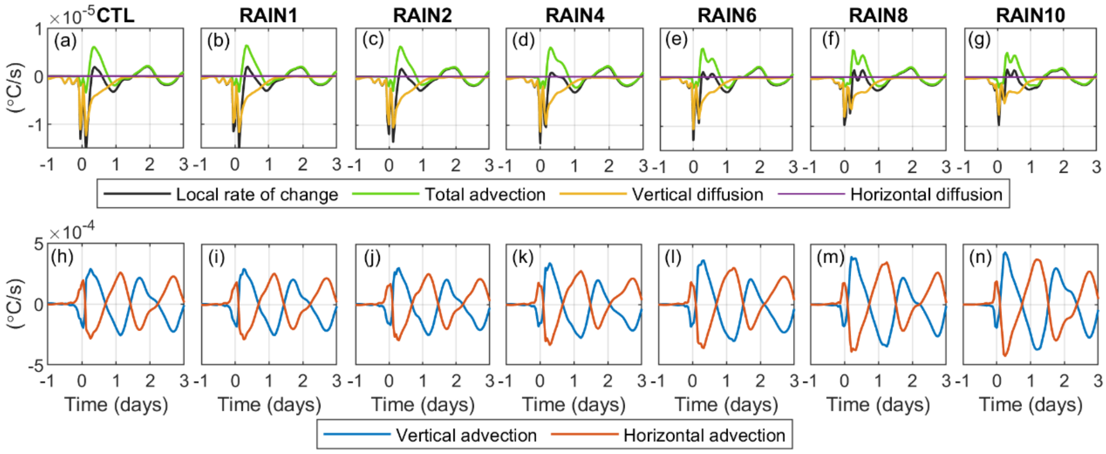

FIG. 8. Time series of the local rate of SST change (black lines in a-g), SST change rate induced by vertical advection (blue lines in h-n) and horizontal advection (red lines in h-n), total advection (green lines in a-g), vertical diffusion (yellow lines in a-g) and horizontal diffusion (purple lines in a-g) at P_{right}. The '0' in x-axis means the approaching time of TC.

Fig. 8 shows the time series of SST budget in 7 experiments with increasing precipitation forcing but constant wind forcing. The horizontal diffusion term is dramatically smaller than other terms and can be omitted in the analysis. The total advection (sum of horizontal and vertical advection) is one order of magnitude smaller than both horizontal and vertical advection since the two terms are out of phase and tend to suppress each other (Fig. 4h-n). The vertical diffusion, i.e., the wind-induced vertical mixing, dominates the wind-induced SST responses during the forced stage and then decays. Then the advection term starts to modulate the SST change. After increasing the precipitation intensity under same wind forcing, both the vertical advection and horizontal advection intensified significantly, especially in RAIN4-RAIN10 (Fig. 8h-n). This indicates more energy was transferred into the deeper ocean and the pressure gradient was modulated, leaving a stronger near-inertial inertial oscillation. A notable signal is that there are two peaks of total advection and SST change rate during 0-1 day in RAIN4-10 (Fig. 8d-g), the lapse rate of vertical diffusion also slowed down at that stage. These features suggest a stronger interaction between the mixed layer and the subsurface layer, as well as the vertical mixing and the upwelling.

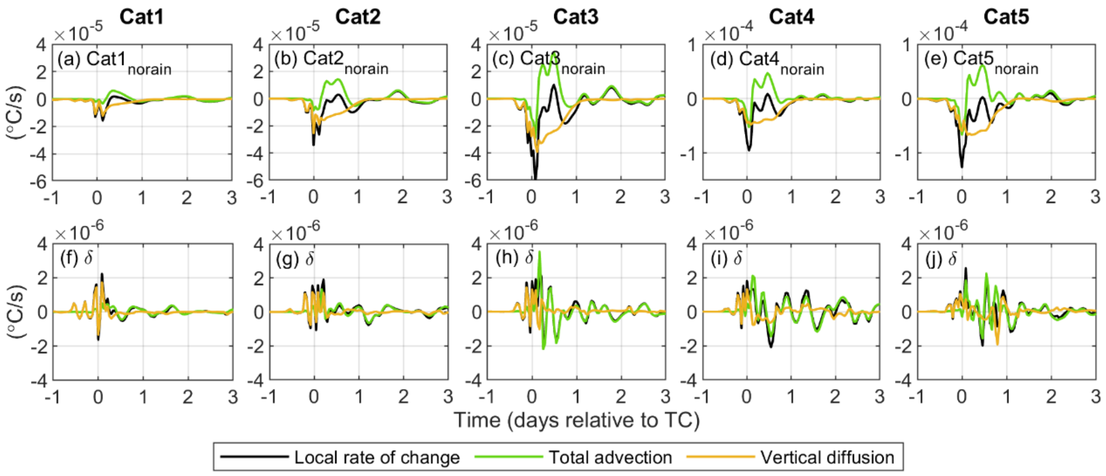

FIG. 9. Time series of the (a-e) local rate of SST change (black lines), SST change rate induced by total advection (green lines) and vertical diffusion (yellow lines in a-g) at P_{right} in 5 experiments with varied TC intensity and without precipitation forcing, as well as the (f-j) precipitation-induced difference. The ‘0’ in x-axis is the approaching time of TC.

In the more realistic experiments, the vertical mixing and total advection intensifies as the TC intensifies due to the larger kinematic energy input by stronger wind forcing (Fig. 9a-e). Considering the freshwater from precipitation forcing, a positive anomaly was added in the local change rate of SST that were originally negative, suggesting a reduction of SST cooling. When TC was weaker than Cat3, the precipitation acts to mainly suppress the vertical diffusion, while the advection process was less modulated (Fig. 9f-h). After TC intensified from Cat3 to Cat5, the precipitation-induced advection become more important, and even exceeds the precipitation-induced vertical mixing (Fig. 9h-j). This transformation indicates the different mechanisms under different wind forcing, which is a result of the competition between the precipitation-induced buoyancy flux and wind effect. Precipitation acts to enhance the upper ocean stability, suppress the vertical mixing when TC is weak and the vertical mixing is not strong enough to break the stratification immediately. Then the effect of precipitation was mainly trapped in mixed layer, and dissipated slowly follow the near-inertial waves. Once the TC is strong enough to break the precipitation-induced stratification, or the vertical mixing is so strong that can redistribute the freshwater before it establishes a stable stratification. Then the freshwater can be transported into deep layer more quickly, thus inducing an intense variation of the near-inertial waves.

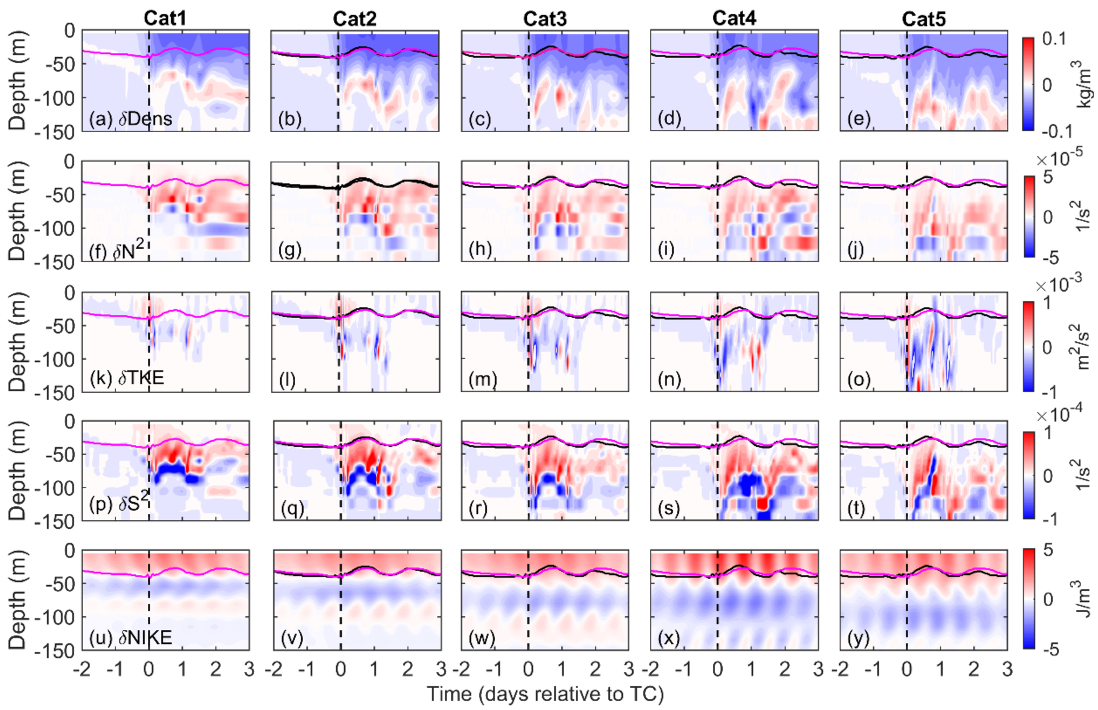

FIG. 10. Collocated time–depth contour plots of differences in (a-e) water density, (f-j) buoyancy frequency, (k-o) turbulence kinetic energy, (p-t) the current shear, and (u-y) the kinetic energy of near-inertial waves at P_{right} induced by precipitation forcing in 5 runs with different TC intensity. The dashed black line indicates the coming time of TC center. The black and magenta solid line indicate the depth of mixed layer in model runs with and without precipitation forcing, respectively.

Fig. 10 shows the time-depth contours of precipitation-induced differences in water density, buoyancy frequency, turbulence kinetic energy and the kinetic energy of near-inertial waves at P_{right}. There is a slightly shallower mixed layer induced by precipitation, as both temperature and salinity stratification were modified by precipitation. The freshwater dilutes surface salinity, reduce the water density and increases the buoyancy frequency, resulting in a larger NIKE in the surface layer. The difference in TKE forms a V-shaped band with positive anomaly above negative centers, indicating that more vigorous turbulent mixing is confined to a shallower layer due to the suppression of stronger stratification. Stronger current shear was caused above 100 m in Cat1 runs, which is similar with Steffen et al., (2020). Consequently, less cold water is entrained into the mixed layer, resulting in a weaker SST cooling after the passage of TC. The NIKE exhibited a significant increase in the upper layer accompanied with a slight decrease in the deep layer. These signals provide evidence that, under the forcing of precipitation, more energy is trapped in upper layer while less energy penetrates into deep layer, leaving a weaker vertical motion and NIWs in deep layer.

Two fundamental signals affected by precipitation are identified: the increased stability induced by freshwater flux and the shallowing of mixed layer. Here arises another question: which is the process by which precipitation induces surface warming? A precipitation-induced shallow mixed layer (less than 20 m depth) was observed in Price (1979), which found that this layer can be destroyed and merged quickly under the effect of wind-driven entrainment. Existing studies indicate that a shallower mixed layer results in stronger surface cooling under the same wind forcing (Zhao and Chan 2017), primarily due to the deeper penetration depth of vertical mixing which can entrain more cold subsurface water into the mixed layer. It seems that the precipitation-induced mixed layer has negligible effect or a positive effect on the SST cooling. Therefore, the increased upper ocean stability is the key factor that contributes to the precipitation-induced SST warming. The fresher surface layer means a light and stable surface layer since the salinity gradient from this fresh layer to deeper layer became larger, which may take more kinematic energy to break through. The increased static stability acts to prevent the vertical mixing from entraining cold water into surface layer, thus inhibiting the cooling in mixed layer. This is a positive factor for the TC development and has been addressed in several studies (Jacob and Koblinsky 2007; Wang et al. 2011; Balaguru et al. 2012; Neetu et al. 2012; Jourdain et al. 2013; Rudzin et al. 2017; Steffen and Bourassa 2018; Rudzin et al. 2019; Hlywiak and Nolan 2019).

d. Nonlinear responses

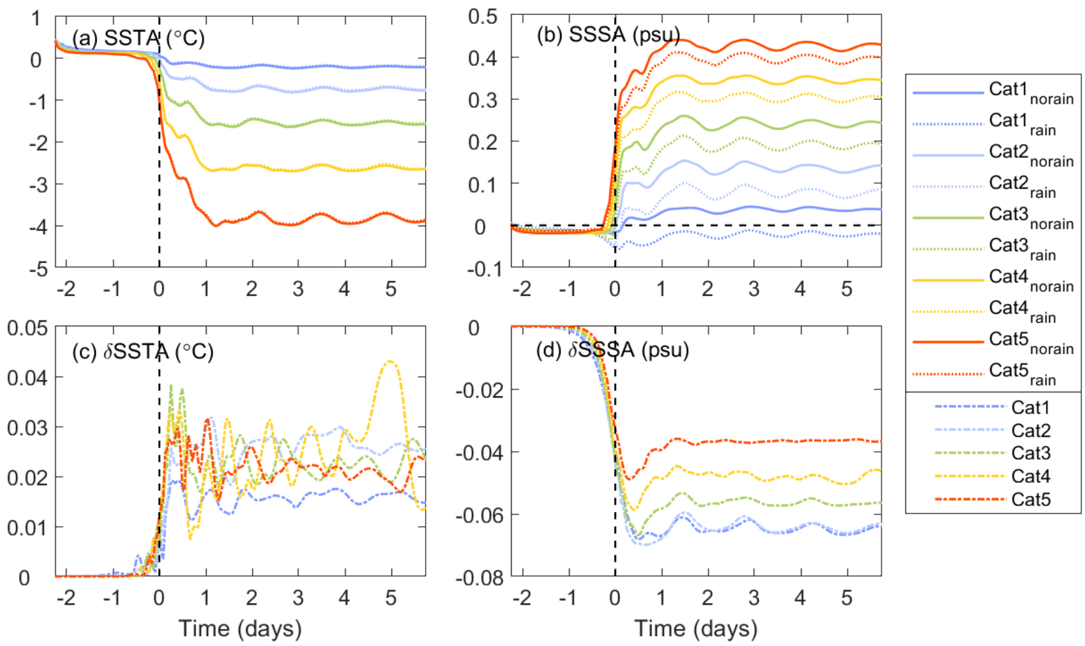

FIG. 11. Time series of (a) SST anomalies, (b) SSS anomalies, and (c-d) precipitation-induced difference of SSTC and SSS anomalies during the whole simulation period at P_{right} i.e., the location at the right side of TC track with a radius of RMW. The '0' in x-axis indicates the approaching time of TC. Different colors indicate different experiments with different initial TC vortex intensity.

Fig. 11 shows the time evolution of the SSTA, SSSA and the difference of SSTA and SSSA induced by precipitation at the radius of RMW at the right side of TC track. The precipitation-induced relative-warming in Cat1 runs occurred earlier than that in other runs (Fig. 11c), suggesting that the precipitation may be important in weak TC cases. In terms of the forced stage, the precipitation-induced warming was not linearly correlated with TC intensity, as the Cat2 and Cat3 runs has a stronger relative warming than Cat4 and Cat5 runs (Fig. 11c, Table3). Even in the relaxation stage, the precipitation-induced warming was not linearly correlated with precipitation (Table 3).

Table 3. Precipitation-induced difference of SST and SSS in 10 experiments. The ‘relaxation stage’ is the period after forced stage, which is typically 5-10 days (Price et al., 1994).

	δSST		δSSS	
	Forced stage	Relaxation stage	Forced stage	Relaxation stage
Cat1_rain - Cat1_norain	0.0145	0.0159	-0.0624	-0.0648
Cat2_rain - Cat2_norain	0.0231	0.0261	-0.0642	-0.0640
Cat3_rain - Cat3_norain	0.0231	0.0227	-0.0580	-0.0564
Cat4_rain - Cat4_norain	0.0210	0.0261	-0.0497	-0.0480
Cat5_rain - Cat5_norain	0.0230	0.0212	-0.0410	-0.0367

Similarly, the precipitation-induced freshening of SSS in forced stage was largest at Cat2 runs, and then decreases as TC intensifies (Fig. 11d). TC tends to create a saltier anomaly by entraining the salty water below mixed layer upward (Domingues et al. 2015; Chaudhuri et al. 2019). However, the positive SSS anomaly in Cat1_norain was replaced with a negative SSS anomaly in Cat1_rain (Fig. 11b), suggesting that the dilution effect of precipitation is overwhelmed the effect of vertical mixing when TC is weak. This phenomenon has been observed by satellite observations (Sun et al. 2021; Ruel et al. 2021). The SSSA then progressively becomes saltier as TC intensifies. The precipitation-induced freshening of SSSA enhanced from Cat1 to Cat2 TC, while it decreased significantly after TC exceeds category 2. This suggests that although the precipitation tends to be heavier under stronger TCs, the dominant factor of SSS anomalies was transferred from precipitation to the wind-induced vertical mixing as the TC intensified, particularly when TC exceeds Cat3.

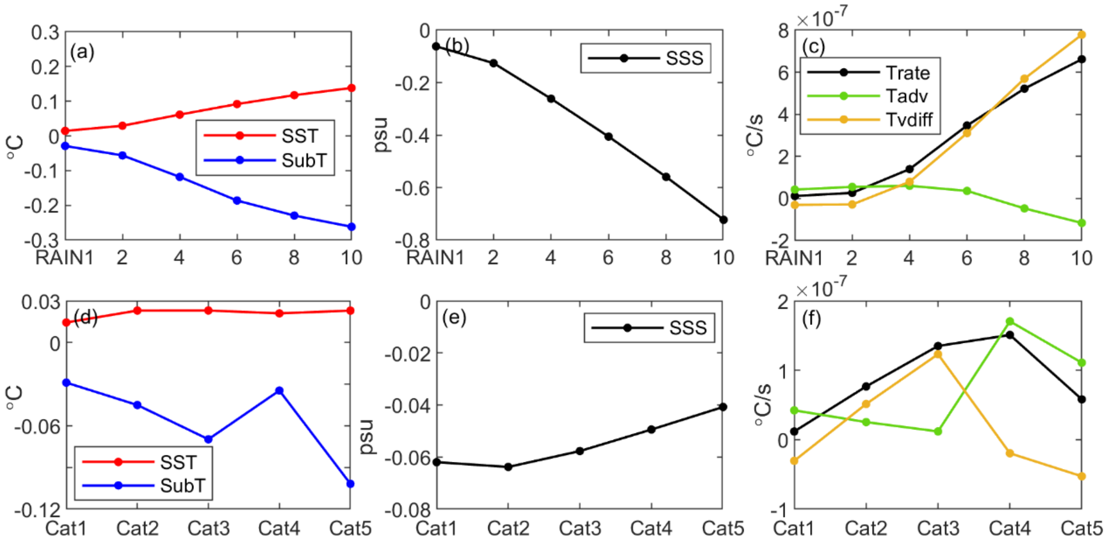

FIG. 12. The dependence of the precipitation-induced difference in SST, subsurface temperature (subT), SSS, and SST tendency terms at a radius of RMW at right side of TC center: (a-c) results in 6 experiments with different precipitation but same wind forcing; (d-f) results in 5 experiments with different precipitation and wind forcing.

To find the key processes that determine the dependence of SST variation on precipitation intensity, we focused on a location at RMW on the right side of TC center. Under the same wind forcing, the precipitation-induced SST warming, the subsurface cooling and the SSS freshening were linearly increased with the precipitation intensity (Fig. 12a, b). The total advection and vertical mixing acts contrast with each other. Note that the total advection acts to support the precipitation-induced warming in RAIN1 and RAIN2 runs. As precipitation intensified, the warming was mainly attributed to the linearly weakened vertical diffusion. When the precipitation and wind forcing is consistent, there is a saturation of precipitation-induced SST warming (Fig. 12d). The subsurface cooling also has a nonlinear dependence with precipitation intensity (Fig. 12f).

Now we can answer the third and fourth questions. There is not a clear saturation of precipitation effect on SST when increasing the precipitation amount while keep the wind forcing as the same. However, the precipitation-induced SST warming levels off as the TC intensified due to the competition between precipitation and wind-driven dynamics. For TCs weaker than Cat3, the weakened vertical mixing is the primary factor that contributes to the relative warming, and it's almost linearly correlated with TC intensity (including both precipitation and wind). For strong TCs (Cat4, Cat5), the local change rate of SST was nonlinear correlated with TC intensity, and the relative warming in controlled by the vertical advection rather than the vertical mixing.

4. Discussion and conclusion

a. Conclusion

By performing sensitivity experiments using an idealized oceanic model under varied TC precipitation and wind forcing, a rightward asymmetry was found in the precipitation-induced relative warm SST anomaly. The maximum relative warming located in the right-rear quadrant because that the precipitation effect was highly coupled with the dynamic processes induced by TC wind forcing, which was rightward biased in the Northern hemisphere. Then we analyzed the vertical response induced by TC precipitation to address the second question. Precipitation can generate a warm-cold-warm anomaly in the surface-subsurface-deep layers, with the magnitude of the subsurface anomaly about three times larger than that of the sea surface. This is a novel result. Then, we can address the third question regarding ocean heat content, as it is highly correlated with the vertical temperature structure in upper ocean. Under the forcing of normal precipitation, the azimuthal mean of TCHP and OHC_{100} within a radius of 400 km increased by about +0.4~+0.5 % under the effect of precipitation, with the maximum located at right-rear quadrant exceeding for +4% for TCHP and 0.8% for OHC^{100}. There is also cancellation of effects, so that across the whole footprint the net change is small. Our study suggests that any potential increase of TC rain rate under the global warming (Guzman and Jiang 2021; Tu et al. 2021) deserves attention since they could enhance the local OHC. Our study presents, for the first time, the nonlinear behavior of the amount of TC precipitation and the oceanic responses. Under the same wind forcing, the vertical mixing weakens progressively as precipitation intensifies, leading to an increasing warm anomaly (or a diminishing cooling response) in SST. However, the precipitation-induced SST warming saturated as both wind forcing and precipitation intensifies. This saturation behavior suggests that the process cannot be considered a simple linear feedback. There will be dampening of the warming as precipitation increases. The saturation can be attributed to the competition between the stabilizing effect of precipitation and wind-induced dynamic modulation, which was also mentioned in previous studies (Brizuela et al. 2022; Ye et al. 2023).

The detailed pathway through which TC precipitation works can be outlined as follows. The direct effect of precipitation is the dilution effect of freshwater. The salinity decreases in a shallow surface layer while the temperature remains unchanged due to the lag in dynamic modulation, resulting in a shallower mixed layer with enhanced stratification. The enhanced stratification prevents vertical mixing from entraining cold water upward, leading to weaker cooling in mixed layer, i.e., a relative warm anomaly associated with precipitation. However, more vigorous turbulent mixing due to the increased current shear amplifies the cold anomaly, which is consistent with Steffen and Bourassa (2020). Additionally, more kinetic energy is trapped in the surface layer, resulting in a stronger (weaker) NIWs in the surface (deeper) layer. The stabilizing effect of precipitation and the enhancement of current shear tend to counteract with each other. Steffen and Bourassa (2020) propose that the horizonal heterogeneity of SST anomalies is caused by the nonlinear interactions between the stratification and current shear. However, our analysis indicates that the stabilizing effect of enhanced stratification is the dominant process through which precipitation affects the upper ocean. This reasoning is supported by the homogeneous SST warm anomaly rather than alternating warm and cold anomalies.

b. Discussion and Limitation

The maximum precipitation-induced SST anomaly, which is +0.02 ℃ under a Cat1 TC case, is considerably lower than the median SST variation induced by TC precipitation report by Jourdain et al. (2013) (0.07 °C), Steffen and Bourassa (2020) (0.3 °C), and Jacob and Koblinsky (2007) (0.2°C~0.5 °C). This may be partly due to the different turbulent ocean mixing parameterizations, given that the strongest signal in Steffen and Bourassa (2020) occurred in model runs with a mixing scheme other than the GLS scheme. Other factors such as the spin-up time of the ocean model, the intensity of TC, the amount of precipitation, and the background oceanic conditions, all may affect the simulations to varying degrees.

A remarkable finding is the homogeneous warm SST anomaly, which is different from the heterogeneous SST anomaly reported in previous studies for real TC cases. Our idealized framework gives a cleaner and novel signal that precipitation causes warm SST anomaly. However, the previous studies on real TC cases demonstrated the simultaneous appearance of warm and cold SST anomalies induced by precipitation (Jacob and Koblinsky 2007; Steffen and Bourassa 2020). This indicates however that the real effect of precipitation will be modulated and amplified in both directions by the complex background ocean currents in real TC cases. Meanwhile, we also find that the SST cooling was always suppressed by precipitation no matter the TC intensities. Nevertheless, a case study on Typhoon Yutu (2018) suggested that the effect of TC precipitation does not always oppose the wind stress effect (Ye et al. 2023). It was found that under the same wind stress forcing (0.14 N/m^2), weak precipitation (rain rate <6.99 mm/h) can enhance the SST cooling, while heavy precipitation (>=10.37 mm/h) can even overwhelm the cooling effect of wind forcing. This contradicts our analysis and may be due to the background ocean complexity of the real case and the varying relative intensity between precipitation and wind forcing in our two studies.

There are several limitations in this study. Apart from the TC intensity, other factors, such as the translation speed (Tu et al. 2022) and the environmental vertical wind shear (Jones 1995), can also affect the intensity and spatial distribution of TC precipitation. It's necessary to conduct an air-sea coupled simulation to get a fuller understanding.

Meanwhile, as indicated in previous studies (Huang et al. 2009; Jourdain et al. 2013), we also found that the effect of TC precipitation on temperature is relatively small and even negligible. Meanwhile, in terms of the short time scale and small spatial scale of extreme precipitation events, it’s challenging to detect the effect of precipitation on SST and on the development of TC itself. However, it is undeniable that precipitation's influence on salinity and stratification is present.

Acknowledgments.

This work was supported by the National Natural Science Foundation of China (42176015, 42227901), the Scientific Research Fund of the Second Institute of Oceanography, MNR (JG2309), the Project supported by Southern Marine Science and Engineering Guangdong Laboratory (Zhuhai) (SML2021SP207), the Innovation Group Project of Southern Marine Science and Engineering Guangdong Laboratory (Zhuhai) (311022001), and the Shanghai Typhoon Research Foundation (TFJJ202111).

Data Availability Statement.

The authors declare that the data supporting the findings of this study are available from the corresponding authors on request.

REFERENCES

Alvey, G. R. III, J. Zawislak, and E. Zipser, 2015: Precipitation properties observed during tropical cyclone intensity change. *Mon. Weath. Rev.*, **143**, 4476–4492, https://doi.org/10.1175/MWR-D-15-0065.1.

Alford, M. H., R.-C. Lien, H. Simmons, J. Klymak, S. Ramp, Y. J. Yang, D. Tang, and M.-H. Chang, 2010: Speed and evolution of nonlinear internal waves transiting the South China Sea. *J. Phys. Oceanogr.*, **40**, 1338–1355, https://doi.org/10.1175/2010JPO4388.1.

Balaguru, K., P. Chang, R. Saravanan, L. R. Leung, Z. Xu, M. Li, and J.-S. Hsieh, 2012: Ocean barrier layers' effect on tropical cyclone intensification. *Proc. Natl. Acad. Sci. USA*, **109**, 14343–14347, https://doi.org/10.1073/pnas.1201364109.

——, G. R. Foltz, L. R. Leung, and K. A. Emanuel, 2016: Global warming-induced upper-ocean freshening and the intensification of super typhoons. *Nat. Commun.*, **7**, 13670, https://doi.org/10.1038/ncomms13670.

——, G. R. Foltz, L. R. Leung, J. Kaplan, W. Xu, N. Reul, and B. Chapron, 2020: Pronounced impact of salinity on rapidly intensifying tropical cyclones. *Bull. Am. Meteorol. Soc.*, **101**, E1497–E1511, https://doi.org/10.1175/BAMS-D-19-0303.1.

——, G. R. Foltz, L. R. Leung, and S. M. Hagos, 2022: Impact of rainfall on tropical cyclone-induced sea surface cooling. *Geophys. Res. Lett.*, **49**, e2022GL098187, https://doi.org/10.1029/2022GL098187.

Bond, N.A., M. F. Cronin, C. Sabine, Y. Kawai, H. Ichikawa, P. Freitag, and K. Ronnholm, 2011: Upper ocean response to Typhoon Choi-Wan as measured by the Kuroshio Extension Observatory mooring. *J. Geophys. Res. Ocean.*, **116**, C02031, https://doi.org/10.1029/2010JC006548.

Brizuela, N. G., T. M. S. Johnston, M. H. Alford, O. Asselin, D. L. Rudnick, J. N. Moum, E. J. Thompson, S. Wang, and C.-Y. Lee, 2023: A vorticity-divergence view of internal wave generation by a fast-moving tropical cyclone: Insights from Super Typhoon Mangkhut. *J. Geophys. Res. Ocean.*, **128**, e2022JC019400, https://doi.org/10.1029/2022JC019400

Chang, I., Bentley, M. L. and Shepherd, J. M. 2014: A global climatology of extreme rainfall rates in the inner core of intense tropical cyclones. *Physical Geography,* **35**, 478-496, https://doi.org/10.1080/02723646.2014.964353.

Chaudhuri, D., D. Sengupta, E. D'Asaro, R. Venkatesan, and M. Ravichandran, 2019: Response of the salinity-stratified Bay of Bengal to cyclone Phailin. *J. Phys. Oceanogr*., **49**, 1121–1140. https://doi.org/10.1175/JPO-D-18-0051.1.

Cione, J. J., and E. W. Uhlhorn, 2003: Sea surface temperature variability in hurricanes: implications with respect to intensity change. *Mon. Weather Rev*., **131**, 1783–1796, https://doi.org/10.1175//2562.1.

Cravatte, S., T. Delcroix, D. Zhang, M. McPhaden, and J. Leloup, 2009: Observed freshening and warming of the western Pacific warm pool. *Clim. Dyn*., **33**, 565–589, https://doi.org/10.1007/s00382-009-0526-7.

Domingues, R., and Coauthors, 2015: Upper ocean response to Hurricane Gonzalo (2014): Salinity effects revealed by targeted and sustained underwater glider observations. *Geophys. Res. Lett*., **42**, 7131–7138, https://doi.org/10.1002/2015GL065378.

Durack, P. J., S. E. Wijffels, and R. J. Matear, 2012: Ocean salinities reveal strong global water cycle intensification during 1950 to 2000. *Science*., **336**, 455–458, https://doi.org/10.1126/science.1212222.

Emanuel, K. A., 1995: Sensitivity of tropical cyclones to surface exchange coefficients and a revised steady-state model incorporating eye dynamics. *J. Atmos. Sci*., **52**, 3969–3976, https://doi.org/10.1175/1520-0469(1995)052<3969:SOTCTS>2.0.CO;2.

Guan, S., W. Zhao, J. Huthnance, J. Tian, and J. Wang, 2014: Observed upper ocean response to typhoon Megi (2010) in the Northern South China Sea, *J. Geophys. Res. Oceans*., **119**, 3134– 3157, https://doi.org/10.1002/2013JC009661.

Guzman, O., and H. Jiang, 2021: Global increase in tropical cyclone rain rate. *Nat. Commun*., **12**, 1–8. https://doi.org/10.1038/ s41467-021-25685-2

Held, I. M. and B. J. Soden, 2006: Robust responses of the hydrological cycle to global warming. *J. Clim*., **19**, 5686–5699, https://doi.org/10.1175/JCLI3990.1.

Hlywiak, J., and D. S. Nolan, 2019: The influence of oceanic barrier layers on tropical cyclone intensity as determined through idealized, coupled numerical simulations. *J. Phys. Oceanogr.*, **49**, 1723–1745, https://doi.org/10.1175/JPO-D-18-0267.1.

Huang, P., T. B. Sanford, and J. Imberger, 2009: Heat and turbulent kinetic energy budgets for surface layer cooling induced by the passage of Hurricane Frances (2004), *J. Geophys. Res.*, **114**, C12023, doi:10.1029/2009JC005603.

Hughes, L. A., 1952: On the low-level wind structure of tropical cyclones, *J. Meteorol.*, **9**, 422–428, https://doi.org/10.1175/1520-0469(1952)009<0422:OTLLSO>2.0.CO;2.

Jacob, S.D., and C. J. Koblinsky, 2007: Effects of precipitation on the upper-ocean response to a hurricane. *Mon. Weather Rev.*, **135**, 2207–2225, https://doi.org/10.1175/MWR3366.1.

Jarugula, S. L., and M. J. McPhaden, 2022: Ocean Mixed Layer Response to Two Post-Monsoon Cyclones in the Bay of Bengal in 2018. *J. Geophys. Res. Ocean.*, **127**, e2022JC018874, https://doi.org/10.1029/2022JC018874

Jones, S. 1995: The evolution of vortices in vertical shear. I: Initially barotropic vortices. *Q. J. R. Meteor. Soc.*, **121**, 821–851. https://doi.org/10.1002/qj.49712152406

Jourdain, N.C., M. Lengaigne, J. Vialard, G. Madec, C. E. Menkes, E. M. Vincent, S. Jullien, and B. Barnier, 2013: Observation-based estimates of surface cooling inhibition by heavy precipitation under tropical cyclones. *J. Phys. Oceanogr.*, **43**, 205–221, https://doi.org/10.1175/JPO-D-12-085.1.

Kara, A. B., P. A. Rochford, and H. E. Hurlburt, 2000: An optimal definition for ocean mixed layer depth. *J. Geophys. Res.*, **105**, 16803–16821, https://doi.org/10.1029/2000JC900072.

Leipper, D., and D. Volgenau, 1972: Hurricane heat potential of the Gulf of Mexico. *J Phys Oceanogr.*, **2**, 218–224, https://doi.org/10.1175/1520-0485(1972)002<0218:HHPOTG>2.0.CO;2.

Liu, F., H. Zhang, J, Ming, J. Zheng, D. Tian, and D. Chen, 2020: Importance of Precipitation on the Upper Ocean Salinity Response to Typhoon Kalmaegi (2014). *Water*., **12**, 614, https://doi.org/10.3390/w12020614.

Lloyd, I. D. and G. A. Vecchi, 2011: Observational evidence for oceanic controls on hurricane intensity. *J. Clim*., **24**, 1138–1153, https://doi.org/10.1175/2010JCLI3763.1.

Lonfat, M., F. D. Marks, and S. Chen, 2004: Precipitation distribution in tropical cyclones using the tropical precipitation measuring mission (TRMM) microwave imager: a global perspective. *Mon. Weath. Rev*, **132**, 1645–1660, https://doi.org/10.1175/1520-0493(2004)132<1645:PDITCU>2.0.CO;2

Lu, Y., P. Chen, H. Yu, P. Fang, T. Gong, X. Wang, and S. Song, 2022: Parameterized Tropical Cyclone Precipitation Model for Catastrophe Risk Assessment in China. *J. Appl. Meteor. Climatol*., **61**, 1291–1303, https://doi.org/10.1175/JAMC-D-21-0157.1.

Madala, R. V., and S. A. Piacsek, 1975: Numerical simulation of asymmetric hurricanes on a beta-plane with vertical shear. *Tellus*., **27**, 453–468, https://doi.org/10.3402/tellusa.v27i5.10172.

Neetu, S., M. Lengaigne, E. M. Vincent, J. Vialard, G. Madec, G. Samson, M. R. Ramesh Kumar, and F. Durand, 2012: Influence of upper-ocean stratification on tropical cyclone-induced surface cooling in the Bay of Bengal. *J. Geophys. Res. Ocean*., **117**, C12020, https://doi.org/10.1029/2012JC008433.

Newinger, C., and R. Toumi, 2015: Potential impact of the colored Amazon and Orinoco plume on tropical cyclone intensity. *J. Geophys. Res. Oceans*., **120**, 1296–1317, https://doi.org/10.1002/2014JC010533.

Price, J. F., 1979: Observations of a Rain-Formed Mixed Layer. *J. Phys. Oceanogr*., **9**, 643–649, https://doi.org/10.1175/1520-0485(1979)009<0643:OOARFM>2.0.CO;2

——, 1981: Upper ocean response to a hurricane. *J. Phys. Oceanogr*., **11**, 153–175, https://doi.org/10.1175/1520-0485(1981)011<0153:UORTAH>2.0.CO;2.

——, T. B. Sanford, and G. Z. Forristall, 1994: Forced stage response to a moving Hurricane. *J. Phys. Oceanogr*., **24**, 233–260, https://doi.org/10.1175/1520-0485(1994)024<0233:FSRTAM>2.0.CO;2.

Rudzin, J. E., L. K. Shay, B. Jaimes, and J. K. Brewster, 2017: Upper ocean observations in eastern Caribbean Sea reveal barrier layer within a warm core eddy. *J. Geophys. Res. Oceans*., **122**, 1057–1071, https://doi.org/10.1002/2016JC012339.

——, ——, and B. Jaimes de la Cruz, 2019: The impact of the Amazon–Orinoco river plume on enthalpy flux and air–sea interaction within Caribbean Sea tropical cyclones. *Mon. Wea. Rev*., **147**, 931–950, https://doi.org/10.1175/MWR-D- 18-0295.1.

Shchepetkin, A.F., and J. C. McWilliams, 2005: The regional oceanic modeling system (ROMS): a split-explicit, free-surface, topography-following-coordinate oceanic model. *Ocean Model*., **9**, 347–404, https://doi.org/10.1016/j.ocemod.2004.08.002.

Steffen, J., and M. Bourassa, 2018: Barrier Layer Development Local to Tropical Cyclones based on Argo Float Observations. *J. Phys. Oceanogr*., **48**, 1951–1968, https://doi.org/10.1175/JPO-D-17-0262.1.

——, and ——, 2020: Upper-Ocean Response to Precipitation Forcing in an Ocean Model Hindcast of Hurricane Gonzalo. *J. Phys. Oceanogr*., **50**, 3219–3234, https://doi.org/10.1175/JPO-D-19-0277.1.

Sun, J., G. Vecchi, and B. Soden, 2021: Sea Surface Salinity Response to Tropical Cyclones Based on Satellite Observations. *Remote Sens*., **13**, 420, https://doi.org/10.3390/rs13030420

Tu, S., J. Xu, J. C. Chan, K. Huang, F. Xu, and L. S. Chiu, 2021: Recent global decrease in the inner-core rain rate of tropical cyclones. *Nat. Commun*., **12**, 1–9. https://doi.org/10.1038/s41467-021-22304-y

——, Chan, J. Xu, Q. Zhong, W. Zhou, and Y. Zhang, 2022: Increase in tropical cyclone rain rate with translation speed. *Nat. Commun*., **13**, 7325, https://doi.org/10.1038/s41467-022-35113-8

Tuleya, R. E., M. Demaria, and R. J. Kuligowski, 2007: Evaluation of GFDL and simple statistical model precipitation forecasts for U.S. landfalling tropical storms. *Wea. Forecasting*., **22**, 56–70, https://doi.org/10.1175/WAF972.1.

Wang, X., G. Han, Y. Qi, and W. Li, 2011: Impact of barrier layer on typhoon-induced sea surface cooling. *Dyn. Atmos. Oceans*, **52**, 367–385, https://doi.org/10.1016/j.dynatmoce.2011.05.002.

Warner, J. C., C. R. Sherwood, H. G. Arango, and R. P. Signell, 2005: Performance of four turbulence closure models implemented using a generic length scale method. *Ocean Modell*., **8**, 81–113, https://doi.org/10.1016/j.ocemod.2003.12.003.

Warner, J.C., B. Armstrong, R. He, and J. B. Zambon, 2010: Development of a coupled oceanatmosphere-wave-sediment transport (COAWST) modeling system. *Ocean Model*., **35**, 230–244. https://doi.org/10.1016/j.ocemod.2010.07.010.

Wentz, F. J., L. Ricciardulli, K. Hilburn, and C. Mears, 2007: How much more rain will global warming bring? *Science*., **317**, 233–235, https://doi.org/10.1126/science.1140746.

Wu, R., S. Wu, T. Chen, Q. Yang, B. Han, and H. Zhang, 2021: Effects of Wave–Current Interaction on the Eastern China Coastal Waters during Super Typhoon Lekima (2019). *J. Phys. Oceanogr*., **51**, 1611–1636, https://doi.org/10.1175/JPO-D-20-0224.1.

Xu, J., and Y. Wang, 2010: Sensitivity of tropical cyclone inner-core size and intensity to the radial distribution of surface entropy flux. *J. Atmos. Sci*., **67**, 1831–1852, https://doi.org/ 10.1175/2010JAS3387.1.

Yan, Y., L. Li, and C. Wang, 2017: The effects of oceanic barrier layer on the upper ocean response to tropical cyclones. *J. Geophys. Res. Oceans*., **122**, 4829–4844, https://doi.org/ 10.1002/2017JC012694.

Ye, S., R. Zhang, and H. Wang, 2023: The role played by tropical cyclones-induced freshwater flux forcing in the upper-ocean responses: A case for Typhoon Yutu (2018). *Ocean Modell*., **184**, 102211, https://doi.org/10.1016/j.ocemod.2023.102211.

Zhang, H., H. He, W. Z. Zhang, and D. Tian, 2021: Upper ocean response to tropical cyclones: a review. *Geosci. Lett.*, **8**, 1, https://doi.org/10.1186/s40562-020-00170-8

Zhang, H., 2023: Modulation of Upper Ocean Vertical Temperature Structure and Heat Content by a Fast-Moving Tropical Cyclone. *J. Phys. Oceanogr.*, **53**, 493–508, https://doi.org/10.1175/JPO-D-22-0132.1.

Zhao, X. and J.C.L. Chan, 2017: Changes in tropical cyclone intensity with translation speed and mixed-layer depth: idealized WRF-ROMS coupled model simulations. *Q.J.R. Meteorol. Soc.*, **143**: 152-163, https://doi.org/10.1002/qj.2905